ELSEVIER

Nuclear Physics A580 (1994) 1–14

NUCLEAR PHYSICS A

# Angular-momentum-projected description of the yrast line of dysprosium isotopes ☆

Y. Sun *, J.L. Egido

*Departamento de Física Teórica C-XI, Universidad Autónoma de Madrid, E-28049 Madrid, Spain*

Received 15 March 1994; revised 7 June 1994

**Abstract**

The yrast levels of the dysprosium isotopes with mass numbers ranging from 154 till 164 are investigated up to high angular momentum. In the theoretical analysis we use the angular-momentum-projected Tamm–Dancoff approximation.

We describe energy levels, moments of inertia, gyromagnetic factors and $B(E2)$ transition probabilities. We find a much better agreement with the experiment than in cranking-type calculations. We are able, in particular, to make a quantitative description of the electromagnetic properties of most of the nuclei involved in this calculation.

## 1. Introduction

The interest for high-spin phenomena started more than twenty years ago with the finding of irregularities in the moment of inertia as a function of the angular momentum [1,2]. These irregularities were interpreted in terms of band crossings of the ground band with two-quasiparticle bands built by particles from the intruder orbits [3].

In the past there have been many experimental studies devoted to the high-spin region of well-deformed nuclei. From these studies one has gathered information about energy levels, linking transition probabilities and gyromagnetic factors of many nuclei. These data plotted against the angular momentum (angular frequency) also display some irregularities; some of them are not yet well understood.

☆ Work supported in part by DGICyT, Spain under project PB91-0006.

* Corresponding author. Present address: Department of Physics and Atmospheric Science, Drexel University, Philadelphia, PA 19104, USA.


*SSDI* 0375-9474(94)00289-Y

From the theoretical point of view there have been many studies devoted to the high-spin region of heavy nuclei, most of them within the mean-field approach (see Ref. [4] for a review) and some of them with particle-number projection [5]. Most of these calculations, however, have been done for isolated nuclei or for specific observables. In spite of the large amount of data that has been accumulated in the past, to our knowledge, only few calculations [6–9] have been devoted to a systematic study of the properties along the yrast line of an isotopic chain. In the calculations [7,8], the erbium, ytterbium and hafnium isotopes have been analyzed in the angular-momentum-projected Tamm–Dancoff approximation; the agreement with the experimental data was excellent. In the other [9] calculation the dysprosium isotopes have been studied within the particle-number-projected mean-field approximation. They obtain a qualitative agreement with the experiment, but they are not able, in particular, to describe the irregularities of the electromagnetic properties along the yrast band.

The purpose of this paper is to perform a systematic study of the high-spin properties of the Dy isotopes in a theory beyond mean field. We go beyond the usual mean-field approach in two aspects: first, by taking into account two- and four-quasiparticle states in the variational process, and second, by projecting them onto good angular momentum. These two features are the main points to make the right description of the band crossings, and therefore, of most of the irregularities observed along the yrast band. The inclusion of two- and four-quasiparticle bands is important to describe the excited bands properly; the angular-momentum projection is necessary to allow the bands to interact at fixed angular momentum and not at a given angular frequency as in the cranking model. These types of approximations [10,11] have been performed in the past to study the energy levels of the erbium, ytterbium and hafnium isotopes [7,8]. In these works, however, no attention was paid to the electromagnetic properties. Similar approximations have been performed by the Tuebingen group [12–14], mostly for lighter nuclei and selected examples. In Ref. [15], electromagnetic properties have been discussed, but only for the $A = 130$ mass region with two selected nuclei.

We have chosen this isotopic chain because it has been experimentally investigated by several groups [16–24]. Specifically, we analyze the Dy isotopes with mass number 154 up to 164. We studied energy levels, moments of inertia and electromagnetic properties along the yrast band up to angular momentum $34\hbar$.

The paper is organized as follows: In Section 2 the underlying theory is examined and the model hamiltonian and the configuration space used in the calculations are discussed. In Section 3 the numerical results are shown and compared with the experimental data; in Subsection 3.1 the energy levels and in Subsection 3.2 the electromagnetic properties. The article ends with the conclusions in Section 4.

## 2. Theory

In this section we briefly describe the theory we use in the calculations. A more detailed description can be found in Refs. [10,11,7].

The physics we want to describe correspond to the high-angular-momentum states of a well-deformed nucleus, with the potential minimum not too far from axial symmetry. To describe high-spin states we know that besides the mean field one has to consider aligned two-quasiparticle bands. Furthermore, if we want the bands to interact at a given spin we have to project the right angular momentum.

Bearing this in mind, the ansatz for the wave function is given by

$$|\sigma, IM\rangle = \sum_{K,\kappa} f_\kappa^\sigma \hat{P}^I_{MK} |\varphi_\kappa\rangle = \sum_\kappa f_\kappa^\sigma \hat{P}^I_{MK_\kappa} |\varphi_\kappa\rangle. \tag{1}$$

The index $\sigma$ labels the states with the same angular momentum and $\kappa$ the basis states. $\hat{P}^I_{MK}$ is an operator which projects the quantum numbers $I$, $M$ [25], and the c-numbers $f_\kappa^\sigma$ are weights of the basis states. Since we restrict ourselves to a basis with axial symmetry, the states $|\varphi_\kappa\rangle$ have a good $K$ quantum number, $K_\kappa$. In the $K$-sum in Eq. (1), therefore, only one term contributes to a given $|\varphi_\kappa\rangle$. In our calculation the states $|\varphi_\kappa\rangle$ are spanned by the set

$$\left\{|\phi\rangle, \quad \alpha^\dagger_{n_i}\alpha^\dagger_{n_i}|\phi\rangle, \quad \alpha^\dagger_{p_i}\alpha^\dagger_{p_j}|\phi\rangle, \quad \alpha^\dagger_{n_i}\alpha^\dagger_{n_j}\alpha^\dagger_{p_k}\alpha^\dagger_{p_l}|\phi\rangle\right\}, \tag{2}$$

with $|\phi\rangle$ a given vacuum to be determined properly (see below) and $\{\alpha_m, \alpha^\dagger_m\}$ the annihilator and creator quasiparticle (qp) operators to this vacuum; the index $n_i$ ($p_i$) runs over selected neutron (proton) states (see below). The index $\kappa$ in Eq. (1) runs over the states of Eq. (2). The suitability of the ansatz of Eq. (1) mainly depends on the election of the reference vacuum $|\phi\rangle$. It will work for well-deformed nuclei where there is a well-deformed minimum and the excited states can be written, to a first approach, as two-quasiparticle states. For soft nuclei it will certainly not work unless we include many quasiparticle states in the basis.

The restriction to an axially symmetric basis is not appropriate for describing $\gamma$-soft nuclei. Most relatively well-deformed nuclei do have an axially symmetric ground state; at high angular momentum the particle alignment provides some mixing of the $K$ quantum number. Such small triaxilities, however, are accounted for, in a good approximation, by the mixing of $K$ states provided by the ansatz of Eq. (2).

The weights $f_\kappa^\sigma$ are determined by diagonalization of the hamiltonian [1] $H' = H - \lambda N$ in the space spanned by the states of Eq. (1); this leads to the eigenvalue equation (for a given spin $I$)

$$\sum_{\kappa'} (H'_{\kappa\kappa'} - E_\sigma \mathcal{N}_{\kappa\kappa'}) f^\sigma_{\kappa'} = 0, \tag{3}$$

and the normalization is chosen such that

$$\sum_{\kappa\kappa'} f^\sigma_\kappa \mathcal{N}_{\kappa\kappa'} f^{\sigma'}_{\kappa'} = \delta_{\sigma\sigma'}. \tag{4}$$

[1] The inclusion of the $\lambda N$ terms in the diagonalization ensures, to first-order perturbation theory, the right particle number on the average for the states (1).

The hamiltonian and norm overlaps are given by

$$H'_{\kappa\kappa'} = \langle \varphi_\kappa | \hat{H}' \hat{P}^I_{K_\kappa K'_{\kappa'}} | \varphi_{\kappa'} \rangle,$$
$$\mathcal{N}_{\kappa\kappa'} = \langle \varphi_\kappa | \hat{P}^I_{K_\kappa K'_{\kappa'}} | \varphi'_\kappa \rangle. \tag{5}$$

It should be noted that, instead of the $\delta_{\kappa\kappa'}$ in a conventional eigenvalue equation, the $\mathcal{N}_{\kappa\kappa'}$ matrix appears in Eq. (3) because of the non-orthogonality of our projected basis.

In the numerical application we use the pairing (monopole and quadrupole) plus quadrupole force [11],

$$\hat{H} = \hat{H}_0 - \tfrac{1}{2}\chi \sum_\mu \hat{Q}^\dagger_\mu \hat{Q}_\mu - G_M \hat{P}^\dagger \hat{P} - G_Q \sum_\mu \hat{P}^\dagger_\mu \hat{P}_\mu, \tag{6}$$

where $\hat{H}_0$ is the spherical single-particle shell-model hamiltonian. The quadrupole $\hat{Q}_\mu$, the monopole-pairing $\hat{P}$ and the quadrupole-pairing $\hat{P}_\mu$ operators are given by

$$\hat{Q}_\mu = \sum_{k,l} (Q_\mu)_{kl} c^\dagger_k c_l, \quad \hat{P} = \tfrac{1}{2} \sum_k c_k c_{\bar{k}}, \quad \hat{P}_\mu = \tfrac{1}{2} \sum_{k,l} (Q_\mu)_{kl} c_k c_l, \tag{7}$$

with $\hat{Q}_\mu = r^2 Y_{2\mu}$. The matrix elements of the $\hat{Q}_\mu$ between different shells are neglected [11]. The strength of the quadrupole force $\chi$ is adjusted such that the known quadrupole deformation parameters $\epsilon_2$ are obtained [26] as a result of the Hartree–Fock–Bogoliubov self-consistent procedure. The monopole-pairing-force constants $G_M$ are adjusted to give the known energy gaps; we use the value

$$G_M = \left(20.12 \mp 13.13 \frac{N-Z}{A}\right) A^{-1}, \tag{8}$$

where the minus (plus) sign applies to neutrons (protons). The strength parameter $G_Q$ for quadrupole pairing is simply taken to be proportional to $G_M$. The proportionality constant varies slightly from nucleus to nucleus as to reproduce the $\nu i_{13/2}$ band crossing at the right place; in the present calculation, on the average, it turns out to be around 0.16.

## 3. Results

To diagonalize the hamiltonian matrix of Eq. (3), first we have to determine the basis states of Eq. (2). The vacuum $|\phi\rangle$ is determined by the diagonalization of a deformed Nilsson hamiltonian and a subsequent BCS calculation – it also provides the chemical potentials $\lambda_p$ and $\lambda_n$ entering into $H'$. In the deformed single-particle calculation we used the standard Nilsson scheme [27]. For lighter isotopes ($^{154}$Dy and $^{156}$Dy), the actual strength of the spin–orbit term seems to be too weak. A slight adjustment in Nilsson parameters is made for neutron major shell 6 and proton major shell 5 according to Ref. [28]; the same adjustment has also been made in early works [7,8]. For the configuration space we take three major shells, $N = 4$, 5 and 6 for neutrons and $N = 3$, 4 and 5 for protons. In the calculations, the

multi-quasiparticle basis selection is carried out in $N = 6$ neutrons and $N = 5$ protons. An energy cutoff (typically 2.5 MeV for a qp pair) has been introduced to take out levels far away from the Fermi level. In this way, only those from the intruder orbits, $i_{13/2}$ neutrons and $h_{11/2}$ protons, are usually selected. The size of the basis, in which the hamiltonian is diagonalized, is typically 50.

### 3.1. Energy levels

To make a comparison with the experiment it is customary to define the rotational frequency $\hbar\omega$ as

$$\omega(I) = \frac{dE(I)}{dI}. \tag{9}$$

In a rotational band, $\hbar\omega$ is half the transition energy along the band. In these nuclei we do not expect an agreement as good as the one found in earlier calculations [7,8] for other isotopes, because the Dy isotopes are not as good rotors as the Er, Yb and Hf isotopes investigated in those papers. As we will see this specially applies for the $^{154-156}$Dy nuclei.

In Fig. 1 we present the rotational frequency versus the angular momentum for the Dy isotopes. The first band crossing, caused by a $i_{13/2}$ neutron aligned band, is well reproduced in all nuclei, though our results do show a larger alignment than in the experiment. In the nuclei $^{154-156}$Dy the first backbending is properly reproduced in the calculations, which, however, predict a second backbending in these nuclei at a spin value of about $28\hbar$. Experimentally there is a second backbending in $^{154}$Dy at a spin value of $34\hbar$. The reason for the discrepancy is probably due to the fact that these nuclei tend to become triaxial at high angular momentum; this degree of freedom has not been allowed in our present calculations. An indication of the tendency to the oblaticity of these nuclei could be the experimentally observed decrease of the $B(E2)$ transition probabilities at high spin (see Fig. 3). In the nucleus $^{158}$Dy the experimental and theoretical results are in good agreement; they predict a backbending (in the experiment upbending) at angular momentum around $16\hbar$. In $^{160-162}$Dy there is no experimental data above the point where the backbending is expected to happen; in $^{164}$Dy the agreement between theory and experiment is very good.

Another important magnitude in high-spin physics is the moment of inertia; it is defined by

$$\mathcal{J} = I/\omega. \tag{10}$$

In Fig. 2 we present the calculated moments of inertia (circles) and the experimental ones (squares). At low spins, with the exception of $^{154}$Dy which is known to be a transitional nucleus, we find a good agreement with the experiment. At medium spins, we are able to describe properly the first backbending caused by the alignment of a $\nu i_{13/2}$ pair (in $^{158}$Dy we get a stronger backbending). Concerning the second irregularity caused by the alignment of a $\pi h_{11/2}$ pair, considering the experimental moments of inertia, it only appears in $^{154}$Dy at a spin value of $34\hbar$;

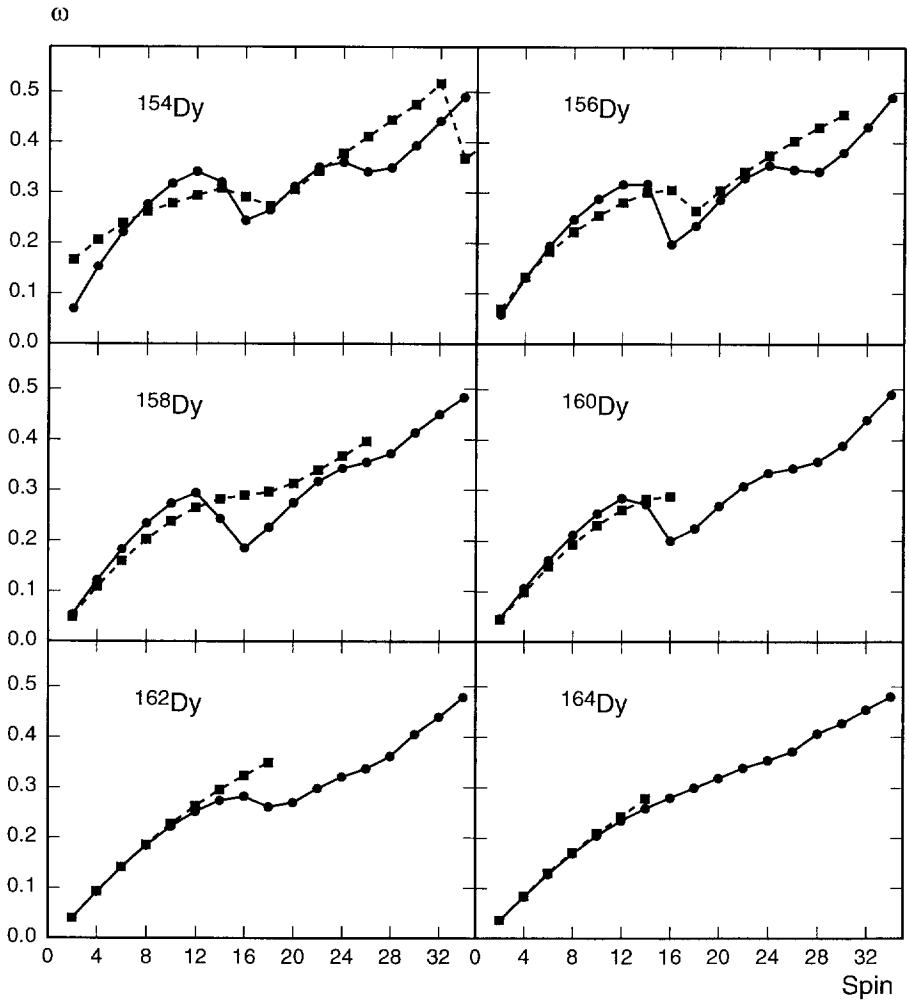


Fig. 1. The theoretical (circles) and experimental (squares) angular frequencies versus the angular momentum for the Dy isotopes.

the other nuclei do not show any, at least in the observed spin range. Theoretically, however, we obtain it in the nuclei $^{154}$Dy and $^{156}$Dy; the possible reason for this disagreement has been discussed above.

### *3.2. Electromagnetic properties*

One of the advantages of using angular-momentum-projected wave functions, as compared with mean-field theories, is that they are laboratory wave functions and can be used directly to calculate observables.

The reduced transition probabilities $B(EL)$ from initial state $(\sigma_i, I_i)$ to final state $(\sigma_f, I_f)$ are given by

$$B(EL, I_i \to I_f) = \frac{e^2}{2I_i + 1} |\langle \sigma_f, I_f \| \mathscr{Q}_L \| \sigma_i, I_i \rangle|^2 \tag{11}$$

and the reduced matrix elements by

$$\begin{aligned}
&\langle \sigma_f, I_f \| \mathscr{Q}_L \| \sigma_i, I_i \rangle \\
&\quad = \sum_{\kappa_i, \kappa_f} f^{\sigma_i}_{\kappa_i} f^{\sigma_f}_{\kappa_f} \sum_{M_i, M_f, M} (-)^{I_f - M_f} \begin{pmatrix} I_f & L & I_i \\ -M_f & M & M_i \end{pmatrix} \\
&\qquad \times \langle \varphi_{\kappa_f} | \hat{P}^{I_f}_{K_{\kappa_f} M_f} \mathscr{Q}_{LM} \hat{P}^{I_i}_{K_{\kappa_i} M_i} | \varphi_{\kappa_i} \rangle \\
&\quad = 2 \sum_{\kappa_i, \kappa_f} f^{\sigma_i}_{\kappa_i} f^{\sigma_f}_{\kappa_f} \sum_{M', M''} (-)^{I_f - K_{\kappa_f}} (2I_f + 1)^{-1} \begin{pmatrix} I_f & L & I_i \\ -K_{\kappa_f} & M' & M'' \end{pmatrix} \\
&\qquad \times \int d\Omega \mathscr{D}^{I_i}_{M'' K_{\kappa_i}}(\Omega) \langle \varphi_{\kappa_f} | \mathscr{Q}_{LM'} \hat{R}(\Omega) | \varphi_{\kappa_i} \rangle .
\end{aligned} \tag{12}$$

To obtain this expression we have made use of some well-known properties of the $\mathscr{D}^I_{MK}$ functions, which can be found, for example, in Section 4.6 of the book by Edmonds [29].

Here we are interested in transitions along the yrast line, i.e. E2 transitions from $I_i = I$ to $I_f = I - 2$. To display the deviations from a rigid rotor, one usually shows the $B(E2)$ referred to the one of a symmetric rotor of the same deformation; in our case with angular-momentum-projected wave functions, this is equivalent to normalize all transition probabilities by the transition probability $B(E2, 2 \to 0)$. In the calculations we use the effective charges of $1.5e$ for protons and $0.5e$ for neutrons.

In Fig. 3 we display the rates $Q_t(I)/Q_t(2)$ for the Dy isotopes. The transition quadrupole moment $Q_t(I)$ is related to the $B(E2)$ transition probability by

$$Q_t(I) = \left( \frac{16\pi}{5} \frac{B(E2, I \to I - 2)}{\langle I\, 0\, 2\, 0 | I - 2\, 0 \rangle} \right)^{1/2} . \tag{13}$$

If the nucleus would behave as a rigid rotor we would obtain a straight line at the unity. Looking at the experimental values, especially those of the lighter isotopes, we observe large deviations from the rigid-rotor behavior. In the rotational-model limit, the $B(E2)$ transition probabilities are related to the shape parameters $(\beta, \gamma)$. Based on their behavior as the angular momentum increases, the general trend one would expect is the following: at small angular momentum we expect an increase of the $B(E2)$ caused by the reduction in the pairing correlations, followed by a depression due to the band crossing (the wave-function overlap of states $I$ and $I - 2$ is small in this region), and then a recovery and later on a decrease caused by the alignment of more particles. This behavior is, to a large extent, well realized in

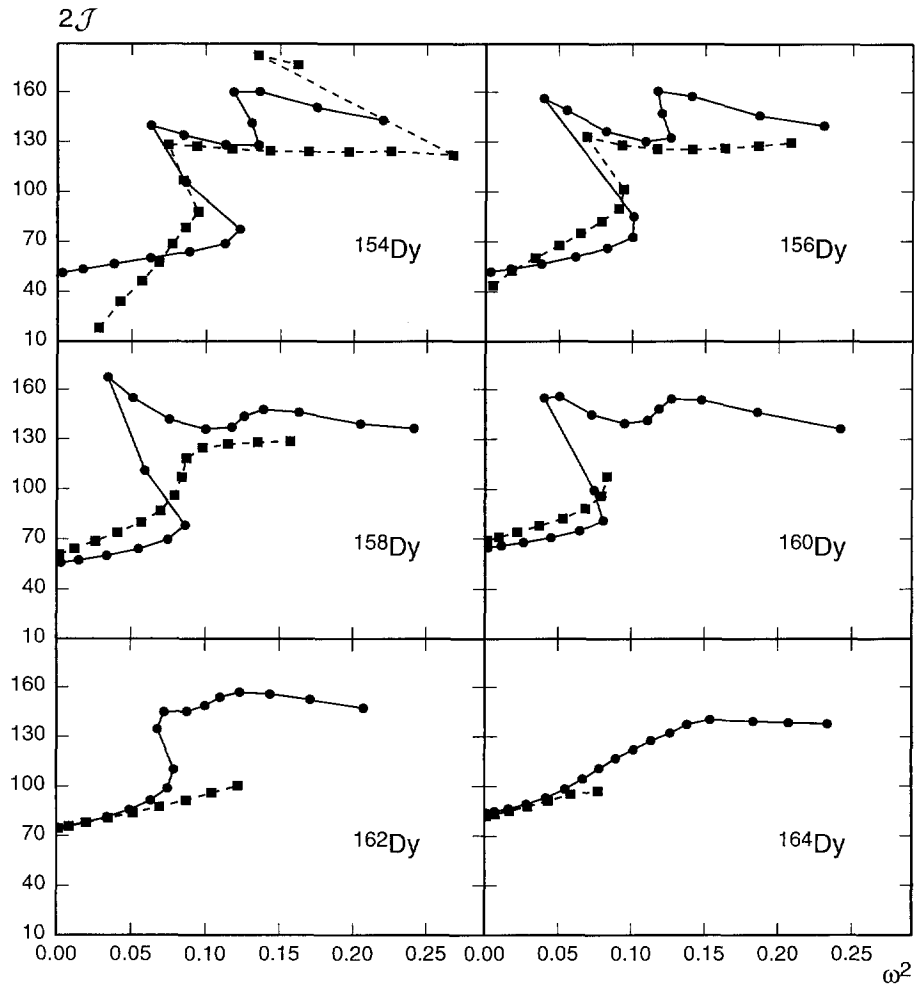


Fig. 2. The theoretical moments of inertia (circles) compared with the experimental values (squares) as a function of the squared angular frequency for the Dy isotopes.

$^{158}$Dy, $^{160}$Dy and $^{162}$Dy. In the nuclei $^{154}$Dy and $^{156}$Dy there are deviations of this behavior at low spins; this could be due to the fact that these nuclei are relatively soft against shape fluctuations. The nucleus $^{164}$Dy also displays some deviations but not as large as the $^{154}$Dy and $^{156}$Dy nuclei. Our theoretical description is able to describe properly most of these features: We obtain a very good description of the nuclei $^{158-160-162-164}$Dy and a fair result for the lighter $^{154}$Dy and $^{156}$Dy, though we are aware that the experimental results do have more structure than the theoretical ones. In particular, we do not get the zigzag behavior at low spins; this behavior is not well understood at the present. Neither do we obtain the steep decrease at spin $30\hbar$ in $^{154}$Dy, which might be due to a softening towards triaxial shapes and which is not explicitly included in our ansatz (2). If we compare our

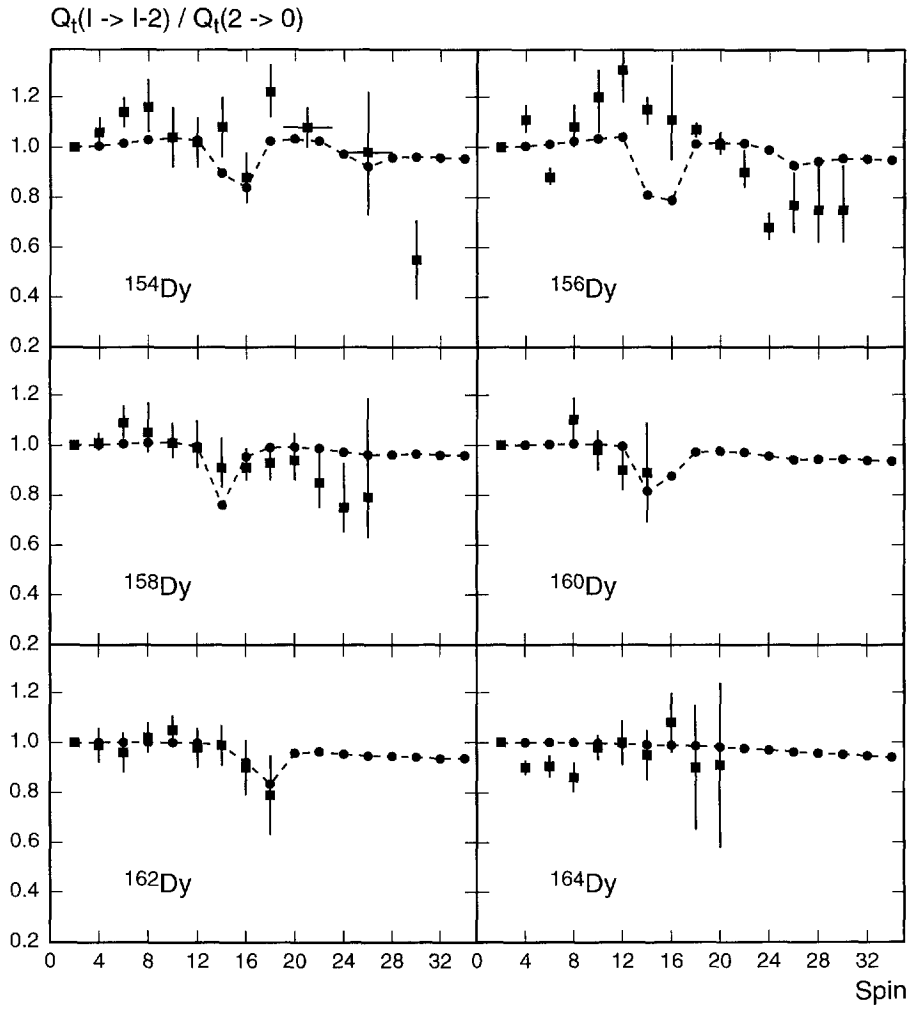


Fig. 3. The theoretical transition quadrupole moments, see Eq. (13), $Q_t(I)/Q_t(2)$ (circles) compared with the corresponding experimental values (squares) as a function of the angular momentum. The experimental values are taken from Ref. [18] for $^{154}$Dy, Ref. [17] for $^{156,158}$Dy and Ref. [23] for $^{160-162-164}$Dy.

calculations with mean-field calculations [9], we observe that in the latter one they obtain almost a constant $B(E2)$ value close to the rigid-rotor value for all $I$ values.

To complete the electromagnetic study of these nuclei we shall now investigate the gyromagnetic factors; these quantities are very sensitive to the alignment processes. The magnetic moment $\mu$ of a state $(\sigma, I)$ is defined by

$$\mu(\sigma, I) = \sqrt{\tfrac{4}{3}\pi}\,\langle \sigma, II \,|\, \mathscr{M}_{10} \,|\, \sigma, II\rangle$$
$$= \frac{(4\pi I)^{1/2}}{[3(I+1)(2I+1)]^{1/2}}\langle \sigma, I \,\|\, \mathscr{M}_1 \,\|\, \sigma, I\rangle. \qquad (14)$$

The operator $\mathscr{M}_{10}$ is given by

$$\mathscr{M}_{10} = \mu_N \sqrt{\frac{3}{4\pi}} \sum_{i=1}^{A} g_l^{(i)} l_z^{(i)} + g_s^{(i)} s_z^{(i)} = \mu_N \sqrt{\frac{3}{4\pi}} \sum_{\tau=p,n} g_l^\tau L_z^\tau + g_s^\tau S_z^\tau, \tag{15}$$

with $\mu_N$ the nuclear magneton, and $g_l$ and $g_s$ the orbital and the spin gyromagnetic factors, respectively.

The gyromagnetic factors $g(\sigma, I)$, $g_p(\sigma, I)$ and $g_n(\sigma, I)$ are defined by

$$g(\sigma, I) = \frac{\mu(\sigma, I)}{\mu_N I} = g_p(\sigma, I) + g_n(\sigma, I), \tag{16}$$

with $g_\tau(\sigma, I)$, $\tau = p, n$, given by

$$g_\tau(\sigma, I) = \frac{1}{[I(I+1)(2I+1)]^{1/2}} \big( g_l^\tau \langle \sigma, I \| J^\tau \| \sigma, I \rangle + (g_s^\tau - g_l^\tau) \langle \sigma, I \| S^\tau \| \sigma, I \rangle \big). \tag{17}$$

These reduced matrix elements are calculated with Eq. (12). In the calculations we use for $g_l$ the free values and for $g_s$ the free values damped [30] by the usual 0.75 factor,

$$g_l^p = 1, \quad g_l^n = 0, \quad g_s^p = 5.586 \times 0.75, \quad g_s^n = 3.826 \times 0.75. \tag{18}$$

Since our configuration space is large enough we do not use any core contribution.

For proton alignment, the contribution $g_l^p \langle \sigma, I \| J^p \| \sigma, I \rangle$ is large and positive and we expect an increasing $g$ factor. For neutron alignment, $g_s^n \langle \sigma, I \| S^n \| \sigma, I \rangle$ is negative and we therefore expect a decreasing $g$ factor. Their behavior can be understood better in the semiclassical mean-field approximation, where one obtains [6]

$$g_\tau = \frac{g_l^\tau \langle \phi_\omega | \hat{J}_x | \phi_\omega \rangle_\tau + (g_s^\tau - g_l^\tau) \langle \phi_\omega | \hat{S}_x | \phi_\omega \rangle_\tau}{\sqrt{I(I+1)}}, \tag{19}$$

with $|\phi_\omega\rangle$ the cranking wave function satisfying the constraint

$$\langle \phi_\omega | \hat{J}_x | \phi_\omega \rangle = \sqrt{I(I+1)} = \mathscr{J}\omega = (\mathscr{J}_p + \mathscr{J}_n)\omega. \tag{20}$$

$\mathscr{J}_p$ ($\mathscr{J}_n$) is the proton (neutron) contribution to the total moment of inertia and $\mathscr{J}_\tau$ is defined by $\mathscr{J}_\tau = \langle \phi_\omega | \hat{J}_x | \phi_\omega \rangle_\tau / \omega$. Taking into account these expressions the proton and neutron $g$ factors can be written as

$$g_p = \frac{\mathscr{J}_p}{\mathscr{J}_p + \mathscr{J}_n} + (g_s^p - g_l^p) \frac{\langle \phi_\omega | \hat{S}_x | \phi_\omega \rangle_p}{\sqrt{I(I+1)}},$$

$$g_n = g_s^n \frac{\langle \phi_\omega | \hat{S}_x | \phi_\omega \rangle_n}{\sqrt{I(I+1)}}. \tag{21}$$

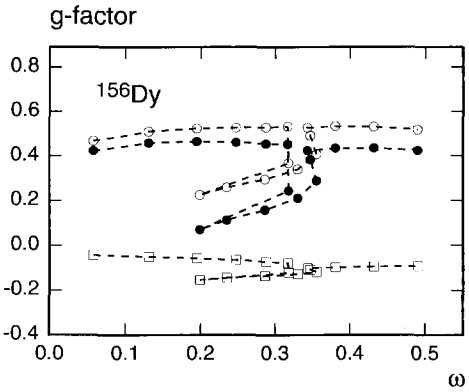


Fig. 4. The theoretical $g$ factors (full circles) as a function of the angular frequency for the nucleus $^{156}$Dy. Proton (open circles) and neutron (open squares) contributions are given separately.

The dominant term in $g_p$ is the first one, which is constant for a rigid rotor and behaves like $Z/A$. Concerning $g_n$, we see that it is much smaller than $g_p$ and negative. A neutron alignment provides a more negative value of $g_n$ and a *decrease* of $g_p$ (through the increase of $\mathcal{J}_n$ in the denominator of the first term of $g_p$). Both effects together account for the observable *decrease* of the total gyromagnetic factor. A proton alignment, on the other hand, produces an *increase* of $g_p$, both through the first and second term, while $g_n$ should change very little. The overall effect is an *increase* of the total $g$ factor. To illustrate these effects, we show in Fig. 4 as an example, the gyromagnetic factors of the nucleus $^{156}$Dy as a function of the angular frequency. Up to $I = 12\hbar$ ($\hbar\omega \approx 0.32$ MeV), $g_n$ and $g_p$ remain rather constant: $g_n$ ($g_p$) slightly decreases (increases) as it corresponds to a collective rotation. For $I = 14\hbar$ and $I = 16\hbar$ we observe a decrease in both $g_n$ and $g_p$, which, as discussed above, can only be caused by neutron alignment. For $I$ values $18\hbar$, $20\hbar$ and $22\hbar$ we find an smooth increase of $g_n$ and $g_p$, of a rather collective character. For $I = 26\hbar$ and $28\hbar$ we see a sharp increase in $g_p$ and an smooth behavior of $g_n$; this situation we interpret as proton alignment. Finally, for $I = 30\hbar$, $32\hbar$ and $34\hbar$ we have collective motion again. Experimentally one only observes the total $g$ factor. But here, as discussed, we observe clearly the mentioned neutron and proton alignment effects in the total $g$ factors.

In Fig. 5 we display the theoretical $g$ factors $g$, $g_p$ and $g_n$ as well as the known experimental $g$ factors, now as a function of the angular momentum, for the Dy isotopes. In the theoretical values we observe a strong neutron alignment in the nuclei $^{154-156-158-160}$Dy around $I = 14\hbar$ and to a minor extent in the nucleus $^{162}$Dy. In the nucleus $^{164}$Dy we do not find any neutron alignment. These results are confirmed by the experimental results in $^{154}$Dy and $^{158}$Dy with which we have a very good agreement. Concerning the proton alignment, we observe a sharp change in the slope of the $g$ factors of the nuclei $^{154-156}$Dy around $I = 24\hbar$. In the nuclei $^{158-160}$Dy there could be a slight proton alignment. Unfortunately, there is

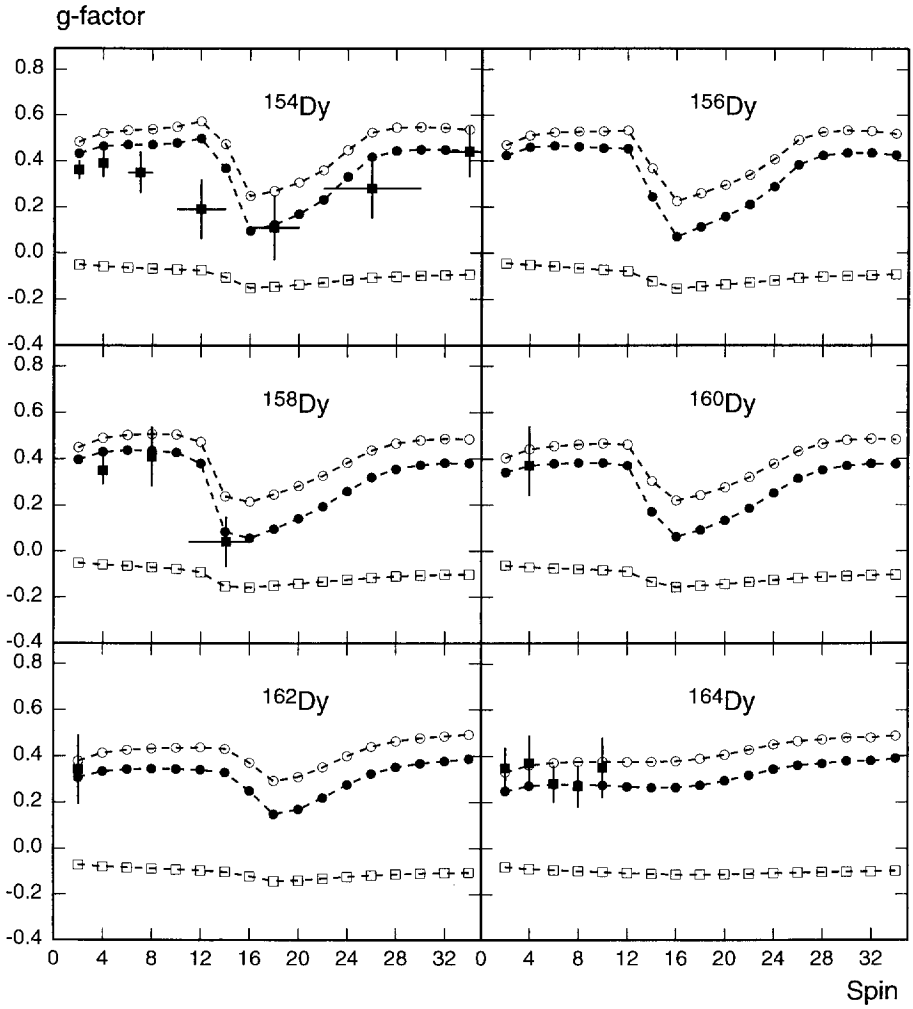


Fig. 5. The theoretical $g$ factors (full circles) compared with the experimental values (open circles) as a function of the angular momentum. Proton (open circles) and neutron (open squares) contributions are given separately. The experimental values are taken from Ref. [24] for $^{154}$Dy, Ref. [16] for $^{158}$Dy, Ref. [19] for $^{162}$Dy and Ref. [21] for $^{164}$Dy.

no experimental data at high spin values to compare with. The only nucleus for which there is experimental data at high spin (with very large error bars) is in $^{154}$Dy [24]. This data would confirm proton alignment as the cause of the sharp backbending that appears at spin $34\hbar$. It is important to note that most of our predictions for the $g$ factors are within the experimental error bars. These results are again at variance with the mean-field approximation [9], where one is not able to describe the experimental $g$ factors of $^{154}$Dy and $^{158}$Dy properly.

## 4. Conclusions

We have performed a systematic study of the dysprosium isotopes within the framework of the angular-momentum-projected Tamm–Dancoff theory. We have used the pairing plus quadrupole hamiltonian (quadrupole pairing included) and three oscillator shells $N = 3$, 4, 5 for protons and $N = 4$, 5, 6 for neutrons. Energies, moments of inertia, E2 reduced transition probabilities and gyromagnetic factors have been analyzed.

We obtain a very good overall description of most of the mentioned observables. The theory is especially successful in reproducing the experimental results for electromagnetic observables, this at variance with standard mean-field theories.

One of us (Y.S.) would like to thank K. Hara for valuable discussions and the Spanish Ministerio de Educación y Ciencia for a grant (REF.: SB90 00075189) of the program "Estancias Temporales de Científicos y Tecnólogos Extranjeros en España".

## References

[1] A. Johnson, H. Ryde and J. Sztarkier, Phys. Lett. B34 (1971) 605
[2] A. Johnson, H. Ryde and S. Hjorth, Nucl Phys. A179 (1972) 753
[3] F.S. Stephens and R.S. Simon, Nucl Phys. A183 (1972) 257
[4] A.L. Goodman, Adv. Nucl. Phys., Vol. 11, Eds. J. Negele and E. Voigt (Plenum, New York, 1979)
[5] J.L. Egido and P. Ring, Nucl. Phys. A383 (1982) 189; A388 (1982) 19
[6] J.L. Egido and P. Ring, Nucl. Phys. A423 (1984) 93
[7] K. Hara and Y. Sun, Nucl Phys. A529 (1991) 445
[8] Y. Sun, Ph.D. thesis, Technical University of Munich (1991), unpublished
[9] M.L. Cescato, Y. Sun and P. Ring, Nucl. Phys. A533 (1991) 455
[10] K. Hara and S. Iwasaki, Nucl Phys. A332 (1979) 61
[11] K. Hara and S. Iwasaki, Nucl Phys. A348 (1980) 200
[12] K.W. Schmid, F. Gruemmer and A. Faessler, Phys. Rev. C29 (1984) 291
[13] K.W. Schmid, F. Gruemmer and A. Faessler, Phys. Rev. C29 (1984) 308
[14] K.W. Schmid and F. Gruemmer, Rep. Prog. Phys. 50 (1987) 731
[15] K.W. Schmid, F. Gruemmer E. Hammarén, M. Kyotoku and A. Faessler, Nucl. Phys. A456 (1989) 437
[16] G. Seiler-Clark, D. Pelte, H. Emling, A. Balanda, H. Grein, E. Grosse, R. Kulessa, D. Schwalm, H.J. Wollersheim, M. Haas, G.J. Kumbartzki and K.-H. Speidel, Nucl. Phys. A399 (1983) 211
[17] H. Emling, E. Grosse, R. Kulessa, D. Schwaln and H.J. Wollershein, Nucl. Phys. A419 (1984) 187
[18] F. Azgui, H. Emling, E. Grosse, C. Michel, R.S. Simon, W. Spreng, H.J. Wollershein, T.L. Khoo, P. Chowdhury, D. Frekers, R.V. Janssens, A. Pakkanen, P.J. Daly, M. Kortelahti, D. Schwaln and G. Seiler-Clark, Nucl. Phys. A439 (1985) 573
[19] R.G. Helmer, Nucl. Data Sheets 44 (1985) 659
[20] W.C. Ma, M.A. Quader, H. Emling, T.L. Khoo, I. Ahmad, P.J. Daly, B.K. Dichter, M. Drigert, U. Garg, Z.W. Grabowski, R. Holzmann, R.V.F. Janssens, M. Piiparinen, W.H. Trzaska and T.-F. Wang, Phys. Rev. Lett. 61 (1988) 46
[21] C.E. Doran, A.E. Stuchbery, H.H. Bolotin, A.P. Byrne and G.J. Lampard, Phys. Rev. C40 (1989) 2035
[22] H. Emling, I. Ahmad, P.J. Daly, B.K. Dichter, M. Drigert, U. Garg, Z.W. Grabowski, R. Holzmann, R.V.F. Janssens, T.L. Khoo, W.C. Ma, M. Piiparinen, M.A. Quader, I. Ragnarsson and W.H. Trzaska, Phys. Lett. B217 (1989) 33

[23] H. Emling, Private communication quoted in M.L. Cescato, Y. Sun and P. Ring, Nucl. Phys. A533 (1991) 455
[24] U. Birkental, A.P. Byrne, S. Heppner, H. Hübel, W. Schmitz, P. Fallon, P.D. Forsyth, J.W. Roberts, H. Kluge, E. Lubkiewicz and G. Goldring, Nucl. Phys. A555 (1993) 643
[25] P. Ring and P. Schuck, The nuclear many body problem (Springer, New York, 1980)
[26] I.L. Lamm, Nucl. Phys. A125 (1969) 504
[27] C.G. Andersson, G. Hellstroem, G. Leander, I. Ragnarsson, S. Åberg, J. Krumlinde, S.G. Nilsson and Z. Szymanski, Nucl. Phys. A309 (1978) 41
[28] T. Bengtsson, Nucl. Phys. A512 (1990) 124
[29] A.R. Edmonds, Angular momentum in quantum mechanics (Princeton University Press, Princeton, NJ, 1974)
[30] A. Bohr and B.R. Mottelson, Nuclear structure, Vol I (Benjamin New York, Amsterdam, 1969)